Published by :
https://www.ijert.org/
An International Peer-Reviewed Journal

International Journal of Engineering Research & Technology (IJERT)
ISSN: 2278-0181
Vol. 15 Issue 08 , August - 2026

Synthesis of Hematite (α-Fe_2O_3) Nanoparticles via a Modified Sol-Gel Route and Their Physicochemical Characterization

S.B. Bansod[1], S.S. Kharode, M.J. Pawar[2], A.A. Mohod
Department of Chemistry, Smt. Narsamma Arts, Commerce and Science College,
Kiran Nagar, Amravati India 444606

Abstract - Hematite (α-Fe_2O_3) nanoparticles were synthesized via a modified sol–gel route, an environmentally benign and cost-effective technique for the fabrication of magnetic iron oxide nanomaterials. Ferric chloride ($FeCl_3$) was employed as the precursor, with the reaction pH and temperature carefully regulated to control nucleation and particle growth, followed by calcination of the dried precipitate at 400°C and 500°C. The resulting nanomaterials were systematically characterized using X-ray diffraction (XRD), Fourier transform infrared spectroscopy (FTIR), field emission scanning electron microscopy (FESEM), transmission electron microscopy (TEM), and Brunauer–Emmett–Teller (BET) surface area analysis. XRD patterns confirmed the formation of a single-phase, well-crystallized rhombohedral (hexagonal corundum-type) hematite structure, free from detectable secondary iron oxide phases or impurities, with the average crystallite size increasing from 33 to 37.3 nm upon raising the calcination temperature, consistent with thermally promoted grain growth. FTIR spectra verified the characteristic Fe–O stretching vibrations of the corundum lattice and revealed a marked reduction in surface hydroxyl and adsorbed moisture content at higher calcination temperature. FESEM and TEM analyses showed porous, foam-like agglomerates of predominantly hexagonal nanoparticles (average size ≈ 70 nm) with well-defined grain boundaries and abundant interparticle voids, favorable for gas diffusion and surface-mediated interactions. BET analysis further indicated an increase in specific surface area from 54 to 66 m^2/g with increasing calcination temperature, attributed to enhanced porosity and reduced surface occlusion. These combined structural, morphological, and textural features suggest that sol–gel-derived α-Fe_2O_3 nanoparticles are promising candidates for applications in gas sensing, photocatalysis, and other surface-reactivity-dependent technologies.

Keywords **- Hematite; α-Fe_2O_3; Sol–gel synthesis; Nanoparticles; XRD; Crystallite size; Calcination; BET surface area**

1. INTRODUCTION

Nanotechnology is an interdisciplinary branch of science and technology that focuses on the design, synthesis, characterization, and application of materials with dimensions ranging from 1 to 100 nanometers (nm). At this nanoscale, materials exhibit unique physical, chemical, optical, electrical, and magnetic properties that differ significantly from their bulk counterparts due to quantum confinement effects and the exceptionally high surface-to-volume ratio. These distinctive characteristics have enabled nanotechnology to revolutionize numerous scientific fields, including chemistry, physics, biology, medicine, environmental science, electronics, and materials engineering [1].

Over the past two decades, nanomaterials have become commercially important and are now incorporated into a wide range of industrial and consumer products. Nanotechnology has contributed to the development of advanced coatings, catalysts, sensors, cosmetics, drug delivery systems, energy storage devices, water purification materials, and biomedical diagnostic tools. The growing demand for sustainable and high-performance materials has further accelerated research into environmentally friendly methods for synthesizing nanoparticles [2,3].

Among the various nanomaterials, magnetic nanoparticles (MNPs) have attracted considerable attention because of their remarkable magnetic behavior and multifunctional applications. These nanoparticles exhibit properties such as superparamagnetism, high magnetic susceptibility, high coercivity, low Curie temperature, and excellent magnetic responsiveness, making them suitable for both technological and biomedical applications [4–6]. In the biomedical field, magnetic nanoparticles are widely employed for targeted drug delivery, magnetic resonance imaging (MRI), hyperthermia treatment for cancer, biosensing, and cell separation. In

(This work is licensed under a Creative Commons Attribution 4.0 International License.)

International Journal of Engineering Research & Technology (IJERT)
ISSN: 2278-0181
Vol. 15 Issue 08 , August - 2026

addition, they are extensively used in catalysis, magnetic recording media, environmental remediation, wastewater treatment, and electromagnetic devices because of their excellent chemical stability and recoverability using an external magnetic field [5,6].

Conventional methods for nanoparticle synthesis often require hazardous chemicals, organic solvents, high temperatures, elevated pressures, and prolonged reaction times. These procedures may generate toxic by-products and increase production costs, thereby limiting their environmental sustainability. To overcome these challenges, researchers have increasingly adopted green synthesis approaches, where plant extracts, microorganisms, or naturally occurring biomolecules act as reducing and capping agents in aqueous media. Green synthesis offers several advantages, including reduced toxicity, lower energy consumption, cost-effectiveness, improved biocompatibility, and enhanced environmental safety, making it an attractive alternative to conventional chemical synthesis [7,8].

Among magnetic nanomaterials, iron oxide nanoparticles (IONPs) are one of the most extensively investigated materials owing to their outstanding magnetic, catalytic, and biocompatible properties. Iron oxides play an important role in chemistry, physics, material science, and nanomedicine. Their excellent stability, low toxicity, abundance, and ease of synthesis have made them promising candidates for photocatalysis, environmental cleanup, biomedical imaging, and magnetic separation technologies [9]. However, the performance of iron oxide nanoparticles strongly depends on their particle size, morphology, crystal structure, and size distribution. Therefore, precise control over synthesis parameters such as precursor concentration, pH, reaction temperature, calcination conditions, and capping agents is essential to obtain nanoparticles with desired properties [10–12].

Control of nanoparticle size is particularly important because magnetic behavior changes dramatically as particle dimensions decrease to the nanometer scale. Uniformly distributed nanoparticles exhibit enhanced superparamagnetic behavior, improved saturation magnetization, and superior heating efficiency during magnetic hyperthermia. Moreover, narrow particle-size distribution contributes to better reproducibility, improved catalytic activity, and enhanced surface reactivity, which are crucial for environmental and biomedical applications [13].

Iron oxide naturally exists in three principal crystalline phases: magnetite (Fe_3O_4), maghemite (γ-Fe_2O_3), and hematite (α-Fe_2O_3). Magnetite possesses an inverse spinel cubic structure and exhibits strong ferrimagnetic behavior, whereas maghemite is a metastable ferrimagnetic phase commonly formed through the oxidation of magnetite. Hematite (α-Fe_2O_3) is the most thermodynamically stable iron oxide under ambient conditions and is one of the oldest known naturally occurring minerals, widely distributed in rocks, soils, and ores [13,14].

Hematite crystallizes in a rhombohedral (hexagonal corundum) crystal system with a density of approximately 5.3 g cm^{-3} and a melting point close to 1350°C. It exhibits antiferromagnetic behavior at room temperature with weak ferromagnetism above the Morin transition due to spin canting. Owing to its narrow band gap (approximately 2.0–2.2 eV), chemical stability, corrosion resistance, low cost, and environmental compatibility, hematite has emerged as an attractive semiconductor material for photocatalysis, photoelectrochemical water splitting, gas sensing, pigments, and lithium-ion battery electrodes [14,15].

Furthermore, iron oxide nanoparticles possess an exceptionally high surface-to-volume ratio, resulting in increased surface energy and a greater number of active surface sites. This characteristic significantly enhances adsorption capacity, catalytic efficiency, electron transfer, and interaction with pollutants, making them highly effective materials for the degradation of organic contaminants and other environmental remediation processes [16]. Consequently, the development of controlled and sustainable synthesis strategies for iron oxide nanoparticles continues to be an important area of research in modern nanotechnology.

In the present study, Fe_3O_4 (Hematite) nanoparticles were synthesized using the sol–gel method, an environmentally friendly and cost-effective approach for preparing magnetic nanomaterials. Compared with conventional synthesis techniques, the sol–gel method offers significant advantages by reducing the use of hazardous chemicals, minimizing energy consumption, and simplifying the overall fabrication process. The synthesized nanoparticles have been characterized by X-ray diffraction (XRD), Fourier transform infrared spectroscopy (FTIR), field emission scanning electron microscope (FESEM), transmission electron microscopy (TEM) and BET analysis. XRD results identify hematite phase of iron oxide nanoparticles. The average crystalline size of the nanoparticles increased from 33 to 37.3 nm when the annealing temperature increased from 400°C to 550°C. FTIR technique also confirmed XRD results.

2. EXPERIMENTAL

2.1 Synthesis of Fe_2O_3 Nanomaterials

Fe_3O_4 nanoparticles were synthesized using the sol–gel method under carefully controlled experimental conditions. An aqueous ferric chloride ($FeCl_3$) precursor solution was prepared and transferred to a condenser system. The reaction temperature was maintained at 70°C using a digitally controlled water bath fitted with temperature sensors, ensuring constant thermal conditions throughout the synthesis. Continuous magnetic stirring was employed to achieve homogeneous mixing of the precursor solution and uniform heat distribution.

(This work is licensed under a Creative Commons Attribution 4.0 International License.)

International Journal of Engineering Research & Technology (IJERT)
ISSN: 2278-0181
Vol. 15 Issue 08 , August - 2026

The pH of the reaction mixture was gradually adjusted to 4.0–5.0 by the dropwise addition of 25% aqueous ammonia (NH_4OH). A calibrated digital pH meter was used to continuously monitor the pH, and periodic adjustments were made to maintain the desired range. Maintaining controlled temperature and pH was essential for promoting uniform nucleation, regulating nanoparticle growth, and minimizing particle agglomeration.

The reaction mixture was stirred for 2 hours, after which it was allowed to cool naturally to room temperature. The resulting suspension was centrifuged at 10,000 rpm for 20 minutes to separate the nanoparticles. The precipitated Fe_3O_4 nanoparticles were collected by filtration and washed several times with distilled water to remove unreacted precursors and soluble impurities.

The purified nanoparticles were dried in a hot-air oven at 70°C under controlled conditions to obtain a dry powder. A small fraction of the sample was preserved for Thermogravimetric Analysis (TGA), while the remaining material was calcined separately at 400°C and 500°C in a muffle furnace. Controlled calcination enhanced the crystallinity and structural stability of the synthesized Fe_3O_4 nanoparticles.

2.2 Characterization of synthesized nanomaterials

The synthesized nanoparticles have been characterized by X-ray diffraction (XRD), Fourier transform infrared spectroscopy (FTIR), field emission scanning electron microscope (FESEM), transmission electron microscopy (TEM) and BET analysis.

3. RESULT AND DISCUSSION

3.1 XRD Analysis

The XRD profile depicted in Figure 1 was recorded over the 2θ range of 20°–80° for the synthesized α-Fe_2O_3 samples. Analysis of the peak positions reveals close conformity with the hexagonal (rhombohedral) crystal system characteristic of α-Fe_2O_3. Diffraction maxima observed at 2θ = 24.05°, 33.15°, 35.61°, 40.78°, 49.50°, 53.92°, 62.62°, and 64.02° were indexed to the (012), (104), (110), (113), (024), (116), (214), and (300) crystallographic planes, respectively, consistent with the standard reference pattern (JCPDS Card No. 33-0664). No extraneous diffraction peaks corresponding to secondary Fe_2O_3 polymorphs (e.g., γ-Fe_2O_3) or other impurity phases were detected within the resolution of the technique, thereby confirming the phase-pure formation of hematite (α-Fe_2O_3) in the synthesized samples.

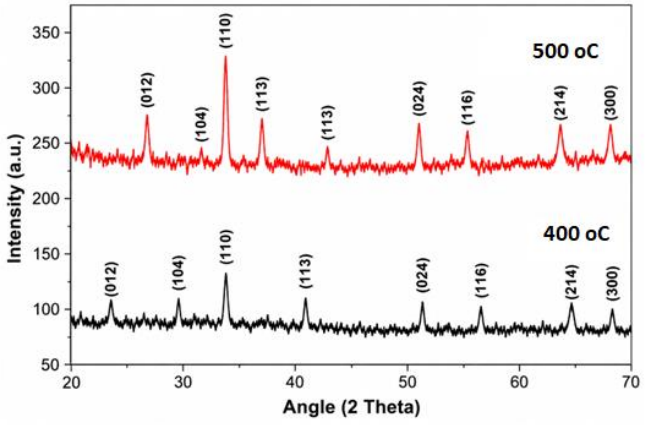

Figure 1 XRD patterns of synthesized Fe_2O_3 nanomaterials.

Among the observed reflections, the (104) peak exhibits the highest relative intensity, suggesting a preferential growth orientation of the crystallites along this particular direction. The narrow and well-defined nature of the diffraction peaks is indicative of a reasonably high degree of crystallinity in the synthesized material. Furthermore, the positions of all observed diffraction maxima correspond closely to the characteristic reflections of the hematite phase (JCPDS Card No. 33-0664). The absence of any supplementary diffraction peaks attributable to secondary phases confirms that the sample exists in a single, phase-pure hematite form.

The average crystallite size of the α-Fe_2O_3 nanoparticles was estimated from the XRD data using the Debye–Scherrer equation:

$$D = \frac{k\lambda}{\beta cos\theta}$$

(This work is licensed under a Creative Commons Attribution 4.0 International License.)

International Journal of Engineering Research & Technology (IJERT)
ISSN: 2278-0181
Vol. 15 Issue 08 , August - 2026

where D denotes the average crystallite size, K is the dimensionless shape factor (typically taken as ~0.9), λ is the wavelength of the incident X-ray radiation (1.54056 Å, corresponding to Cu Kα radiation), β is the full width at half maximum (FWHM) of the diffraction peak (expressed in radians), and θ is the Bragg diffraction angle.

3.2 FTIR Analysis

Fourier Transform Infrared (FTIR) spectroscopy was employed to identify the functional groups and confirm the formation of the Fe–O bonding network in the synthesized iron oxide nanomaterials calcined at 400°C and 500°C, as illustrated in Figure X. The spectra were recorded in the wavenumber range of 4000–400 cm^{-1}.

For the sample calcined at 400°C, a broad absorption band centered at 3434 cm^{-1} is observed, which is attributed to the stretching vibrations of surface-adsorbed hydroxyl groups (–OH) and physisorbed water molecules. A corresponding band at 1633 cm^{-1} arises from the bending (scissoring) vibration mode of molecularly adsorbed H_2O, further confirming the presence of residual surface moisture. Notably, this band is comparatively weaker and shifted to 1631 cm^{-1} in the sample calcined at 500°C, indicating a marked reduction in surface-bound water content as a result of the higher thermal treatment.

The characteristic fingerprint region below 700 cm^{-1} confirms the formation of the hematite (α-Fe_2O_3) phase. For the sample calcined at 400°C, absorption bands appear at 589 cm^{-1} and 417 cm^{-1}, which are assigned to the Fe–O stretching vibrations corresponding to the tetrahedral and octahedral coordination sites of Fe^{3+} within the hexagonal corundum-type lattice, respectively. Upon calcination at 1000°C, these bands become sharper and shift slightly to 598 cm^{-1}, 482 cm^{-1}, and 417 cm^{-1}, reflecting improved lattice ordering and enhanced crystallinity at elevated temperature. The emergence of an additional resolved band at 482 cm^{-1} in the high-temperature sample can be attributed to more complete phase transformation and reduced structural disorder, consistent with the coalescence of nanoparticles and grain growth typically associated with high-temperature annealing.

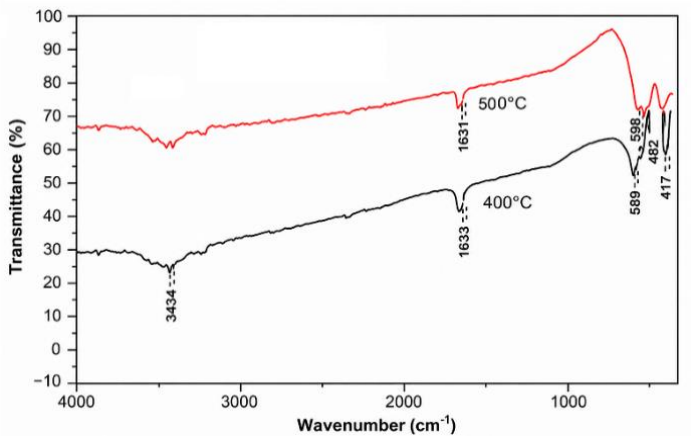

Figure 2. FTIR spectra of Fe_2O_3 nanomaterials.

3.3 Morphological studies

3.3.1 SEM Analysis

The surface morphology of the as-synthesized nanoparticles was examined using field emission scanning electron microscopy. The FESEM micrographs presented in Figure 3 reveal a relatively uniform distribution of the iron oxide nanoparticles [17]. Particle size analysis indicates that the synthesized nanoparticles range from approximately 50 to 90 nm in diameter, with a mean particle size of 70 nm. The particles predominantly exhibit hexagonal morphology and are observed to form foam-like agglomerates displaying a broad size distribution. The formation of voids within the particle assembly can be attributed to the tendency of the nanoparticles to aggregate and coalesce under the elevated temperature conditions employed during hydrothermal synthesis.

Additionally, the micrographs reveal well-defined grain boundaries, indicative of good porosity within the synthesized material [18]. The presence of numerous interparticle void spaces is particularly noteworthy, as such porous architecture may facilitate gas diffusion across the α-Fe_2O_3 surface, thereby potentially enhancing the material's gas-sensing performance [19]. The bulk density of the synthesized particles was determined to be approximately 1 g cm^{-3}, a parameter of considerable significance in governing the enhanced functional properties characteristic of nanoscale materials.

(This work is licensed under a Creative Commons Attribution 4.0 International License.)

International Journal of Engineering Research & Technology (IJERT)
ISSN: 2278-0181
Vol. 15 Issue 08 , August - 2026

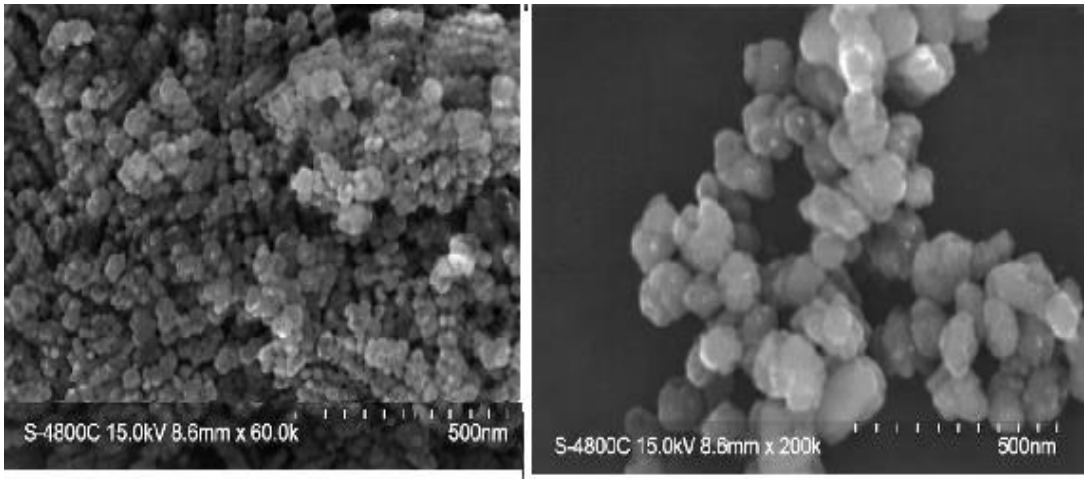

Figure 3. HRTEM images of synthesized Fe_2O_3 nanomaterials.

Furthermore, a discrepancy is observed between the crystallite size determined via X-ray diffraction and the particle size obtained from FESEM analysis. This difference can be rationalized by the fact that XRD-derived crystallite size reflects the dimensions of individual coherently diffracting crystalline domains, whereas FESEM provides a measure of the overall particle size, which may itself comprise multiple such crystalline domains or subunits.

The progressive sharpening and better resolution of the Fe–O vibrational bands with increasing calcination temperature (400°C → 500°C), coupled with the diminishing intensity of the hydroxyl and adsorbed water bands, collectively confirm the enhanced crystallization, phase purity, and reduction of surface defects/moisture in the α-Fe_2O_3 nanostructures at higher thermal treatment.

3.3.2 TEM Analysis

Additional confirmation of the nanoscale architecture of the synthesized materials was obtained through transmission electron microscopy (TEM), with the corresponding micrographs presented in Figure 4(A) and 4(B). The TEM images reveal that the synthesized α-Fe_2O_3 calcined at 400 and 500°C nanoparticles exhibit maximum particle dimensions of approximately 50 nm and 20 nm, respectively, thereby corroborating the nanocrystalline nature of both samples.

The α-Fe_2O_3 nanoparticles display a pronounced tendency toward agglomeration, forming clusters composed of a heterogeneous mixture of morphologies including spherical, dendritic, and occasional flower-like (or petal-like) configurations. This morphological irregularity in the sample may be attributed to the absence of any stabilizing or nucleation-controlling influence during particle growth, allowing for uncontrolled aggregation and non-uniform crystal growth.

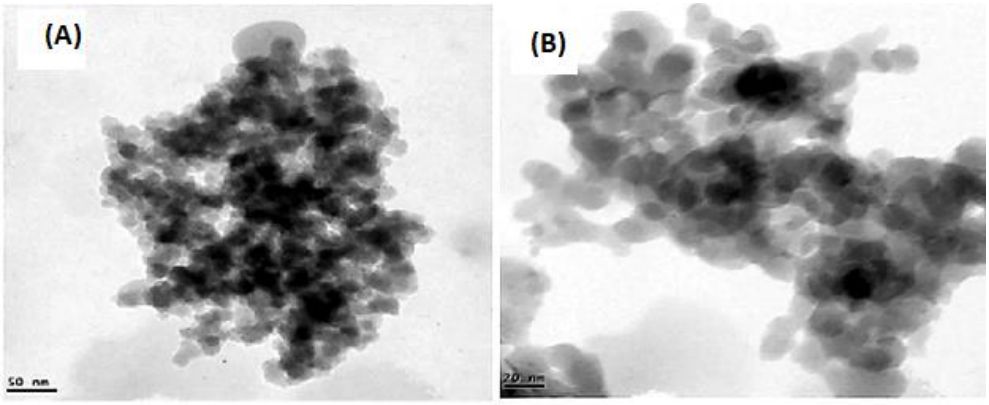

Figure 4. TEM images of synthesized nanomaterials.

Quantitative analysis of particle size distribution from the TEM micrographs indicates that the average diameter of the as-synthesized α-Fe_2O_3 nanoparticles (~20 nm) is notably smaller. This reduction in average particle size is consistent with the trend observed in the corresponding FESEM analysis, thereby validating the reliability and reproducibility of the particle size estimation across the two independent microscopic characterization techniques. The consistency between TEM and SEM results further reinforces the conclusion that silver doping plays a significant role in refining the crystallite size and morphology of the α-Fe_2O_3 nanostructure, which may have important implications for enhancing surface area-dependent properties such as photocatalytic activity and gas-sensing performance.

(This work is licensed under a Creative Commons Attribution 4.0 International License.)

International Journal of Engineering Research & Technology (IJERT)
ISSN: 2278-0181
Vol. 15 Issue 08 , August - 2026

3.4 BET Surface Area Analysis

The specific surface areas of the samples calcined at 400°C, as determined by the Brunauer–Emmett–Teller (BET) method, were found to be 54 m^2/g for the hematite α-Fe_2O_3 sample. Notably, a progressive enhancement in surface area was observed with increasing calcination temperature, reaching a value of 66 m^2/g.

This enhancement in surface area with increasing thermal treatment can be attributed to several possible structural and morphological factors. Elevated calcination temperatures may promote the complete decomposition of residual precursor species, organic remnants, and surface-bound hydroxyl/water molecules, thereby unveiling previously inaccessible micro- and mesoporous domains within the particle framework. Additionally, the thermal energy supplied during calcination may induce further structural reorganization, such as the development of a more open, porous network or an increase in surface roughness at the nanoscale, both of which would contribute to a higher effective surface area accessible to nitrogen adsorption during BET analysis. The evolution of interparticle voids and grain boundary porosity, as also evidenced in the FESEM morphological analysis, may further support this enhanced surface area trend, providing improved pathways for gas diffusion and adsorption a feature of particular relevance to the material's potential application in gas-sensing and catalytic processes.

4. CONCLUSION

In this study, phase-pure α-Fe_2O_3 (hematite) nanoparticles were successfully synthesized via a modified sol–gel method, and the influence of calcination temperature (400°C and 500°C) on their structural, morphological, and textural properties was systematically investigated. XRD analysis confirmed the formation of a single, well-crystallized rhombohedral hematite phase, with all diffraction peaks indexed to the corresponding planes of α-Fe_2O_3 (JCPDS Card No. 33-0664) and no detectable impurity phases. The average crystallite size, calculated using the Debye–Scherrer equation, increased from 33 to 37.3 nm with increasing calcination temperature, reflecting enhanced crystallinity and thermally driven grain growth. FTIR spectroscopy corroborated the XRD findings, confirming the characteristic Fe–O stretching vibrations of the hexagonal corundum lattice and revealing a progressive reduction in surface-adsorbed hydroxyl and water content at higher calcination temperature. FESEM and TEM investigations revealed porous, foam-like agglomerates composed of predominantly hexagonal nanoparticles with an average size of approximately 70 nm, exhibiting well-defined grain boundaries and abundant interparticle voids conducive to gas diffusion. Furthermore, BET surface area analysis demonstrated an increase in specific surface area from 54 to 66 m^2/g with rising calcination temperature, consistent with the development of a more porous microstructure. Collectively, these findings establish the sol–gel method as a simple, reproducible, and environmentally sustainable route for producing high-purity, crystalline α-Fe_2O_3 nanoparticles with tunable crystallite size and surface area. The favorable structural and textural characteristics of the synthesized nanomaterials, particularly their high surface area and porous morphology, underscore their strong potential for application in gas sensing, photocatalysis, environmental remediation, and other surface-reactivity-driven technologies. Future work may focus on evaluating the functional performance of these nanoparticles in targeted applications and further optimizing the synthesis parameters to fine-tune their physicochemical properties.

REFERENCES

[1] Poole CP Jr, Owens FJ. Introduction to Nanotechnology. Hoboken: John Wiley & Sons; 2003.
[2] Rao CNR, Müller A, Cheetham AK. The Chemistry of Nanomaterials. Weinheim: Wiley-VCH; 2004.
[3] Daniel MC, Astruc D. Gold nanoparticles: Assembly, supramolecular chemistry, quantum-size-related properties, and applications. Chem Rev. 2004;104:293–346.
[4] Laurent S, Forge D, Port M, Roch A, Robic C, Elst LV, et al. Magnetic iron oxide nanoparticles: synthesis, stabilization, vectorization and biomedical applications. Chem Rev. 2008;108:2064–2110.
[5] Pankhurst QA, Connolly J, Jones SK, Dobson J. Applications of magnetic nanoparticles in biomedicine. J Phys D Appl Phys. 2003;36:R167–R181.
[6] Lu AH, Salabas EL, Schüth F. Magnetic nanoparticles: synthesis, protection, functionalization, and application. Angew Chem Int Ed. 2007;46:1222–1244.
[7] Iravani S. Green synthesis of metal nanoparticles using plants. Green Chem. 2011;13:2638–2650.
[8] Ahmed S, Ahmad M, Swami BL, Ikram S. A review on plants extract mediated synthesis of silver nanoparticles for antimicrobial applications. J Adv Res. 2016;7:17–28.
[9] Gupta AK, Gupta M. Synthesis and surface engineering of iron oxide nanoparticles for biomedical applications. Biomaterials. 2005;26:3995–4021.
[10] Sun S, Zeng H. Size-controlled synthesis of magnetite nanoparticles. J Am Chem Soc. 2002;124:8204–8205.
[11] Massart R. Preparation of aqueous magnetic liquids in alkaline and acidic media. IEEE Trans Magn. 1981;17:1247–1248.
[12] Cornell RM, Schwertmann U. The Iron Oxides: Structure, Properties, Reactions, Occurrences and Uses. 2nd ed. Weinheim: Wiley-VCH; 2003.
[13] Cullity BD, Graham CD. Introduction to Magnetic Materials. 2nd ed. Hoboken: Wiley-IEEE Press; 2008.
[14] Cornell RM, Schwertmann U. Natural occurrence and crystal chemistry of hematite. In: The Iron Oxides. Wiley-VCH; 2003.
[15] Kay A, Cesar I, Grätzel M. New benchmark for water photooxidation by nanostructured α-Fe_2O_3 films. J Am Chem Soc. 2006;128:15714–15721.
[16] Wang SB, Zhu ZH. Effects of surface area and porosity on nanoparticle adsorption and catalytic performance. J Hazard Mater. 2007;136:482–501.
[17] Khalil M, Yu J, Liu N, Lee RL (2014) Non-aqueous modification of synthesized hematite nanoparticles with oleic acid. Colloids Surf A 453: 7-12.
[18] Cheng W, Xu X, Wu F, Li J (2016) Synthesis of cavity-containing iron oxide nanoparticles by hydrothermal treatment of colloidal dispersion. Mater Lett 164: 210-212.
[19] Wang F, Qin XF, Meng YF, Guo ZL, Yang LX, et al. (2013) Hydrothermal synthesis and characterization of α-Fe_2O_3 Mater Sci Semicond Process 16(3): 802-806.

(This work is licensed under a Creative Commons Attribution 4.0 International License.)